NOISE DUE TO INTERACTION OF BOUNDARY LAYER TURBULENCE

WITH A COMPRESSOR OR A PROPULSOR ROTOR

N. Moiseev, B. Lakshminarayana, D. E. Thompson

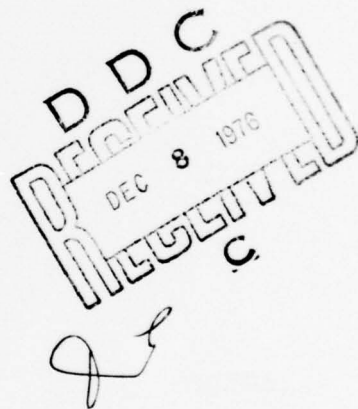The Pennsylvania State University
APPLIED RESEARCH LABORATORY
Post Office Box 30
State College, PA 16801

Approved for Public Release

NAVY DEPARTMENT

NAVAL SEA SYSTEMS COMMAND

REPORT DOCUMENTATION PAGE		READ INSTRUCTIONS BEFORE COMPLETING FORM
1. REPORT NUMBER TM-76-241	2. GOVT ACCESSION NO.	3. RECIPIENT'S CATALOG NUMBER
4. TITLE (and Subtitle) NOISE DUE TO INTERACTION OF BOUNDARY LAYER TURBULENCE WITH A COMPRESSOR OR A PROPULSOR ROTOR.		5. TYPE OF REPORT & PERIOD COVERED Technical Memorandum
		6. PERFORMING ORG. REPORT NUMBER
7. AUTHOR(s) N. Moiseev, B. Lakshminarayana, D. E. Thompson		8. CONTRACT OR GRANT NUMBER(s) N00017-73-C-1418
9. PERFORMING ORGANIZATION NAME AND ADDRESS Applied Research Laboratory P. O. Box 30 State College, PA 16801		10. PROGRAM ELEMENT, PROJECT, TASK AREA & WORK UNIT NUMBERS
11. CONTROLLING OFFICE NAME AND ADDRESS Naval Sea Systems Command Washington, DC 20362		12. REPORT DATE 27 Aug 976
		13. NUMBER OF PAGES 46
14. MONITORING AGENCY NAME & ADDRESS(if different from Controlling Office) SR02391 SR0230191		15. SECURITY CLASS. (of this report) UNCLASSIFIED
		15a. DECLASSIFICATION/DOWNGRADING SCHEDULE

16. DISTRIBUTION STATEMENT (of this Report)

Approved for public release. Distribution unlimited.
Per NAVSEA - 2 June 1976

17. DISTRIBUTION STATEMENT (of the abstract entered in Block 20, if different from Report)

18. SUPPLEMENTARY NOTES

Presented at the AIAA 3rd Aero-Acoustics Conference, Palo Alto, CA, July 20-23, 1976, AIAA preprint.

19. KEY WORDS (Continue on reverse side if necessary and identify by block number)

Boundary Layer   Propulsors
Turbulence   Rotors
Noise
Radiated Sound
Compressors

20. ABSTRACT (Continue on reverse side if necessary and identify by block number)

The radiated sound due to a compressor or propulsor rotating blade row was investigated under various operating conditions and inflows. The propulsor was operated in air with different blade space-to-chord ratios, different flow coefficients and differing turbulence (non-isotropic) inflows. The inflows ingested are: 1) the natural boundary layer on the hub and annulus wall, 2) a tripped boundary layer on the hub, and 3) a fully developed boundary layer on the hub. The turbulence properties were also altered by placing a grid

next page

DD FORM 1473 1 JAN 73   EDITION OF 1 NOV 65 IS OBSOLETE

391007

cont.

at the inlet. The mean velocity profiles, turbulence intensities, length scales, and energy spectra of the inflow were measured, as well as near and far-field acoustic spectra. A parametric investigation of the effect of inflow character-istics on the radiated sound has been made. Several length scales were found to exist simultaneously. The noise due to small scale turbulence seems to depend on, i.e., turbulence velocity normal to the blade divided by the axial length scale. The long eddies are also responsible for discrete tone production.

Abstract: The radiated sound due to a compressor or propulsor rotating
blade row was investigated under various operating conditions
and inflows. The propulsor was operated in air with different
blade space-to-chord ratios, different flow coefficients and
differing turbulence (non-isotropic) inflows. The inflows
ingested are: 1) the natural boundary layer on the hub and
annulus wall, 2) a tripped boundary layer on the hub, and
3) a fully developed boundary layer on the hub. The turbulence
properties were also altered by placing a grid at the inlet. The
mean velocity profiles, turbulence intensities, length scales,
and energy spectra of the inflow were measured, as well as near
and far-field acoustic spectra. A parametric investigation of
the effect of inflow characteristics on the radiated sound has
been made. Several length scales were found to exist simul-
taneously. The noise due to small scale turbulence seems to
depend on, i.e., turbulence velocity normal to the blade divided
by the axial length scale. The long eddies are also responsible
for discrete tone production.

TABLE OF CONTENTS

LIST OF SYMBOLS

ABL	artificial boundary layer
B	number of blades
c	blade chord
C_L	lift coefficient based on cascade mean velocity
$E_{u_i u_j}(k)$	spectrum function of turbulence kinetic energy
FDBL	fully developed boundary layer
k	wave number
L_x, L_θ	axial integral length scale $(T U_x)$ and tangential integral length scale respectively
NBL	natural boundary layer
$\sqrt{\overline{q^2}}$	turbulence velocity (rms value) normal to blade chord
r_T	tip radius of rotor
r, θ, x	radial, tangential and axial coordinates respectively
S	local blade spacing $2\pi r/B$
T	integral time scale
u	fluctuating velocity in the axial direction
U_c	axial mean velocity at mid radius
U_{rel}	$(U_x^2 + U_t^2)^{1/2}$, flow velocity relative to rotor
U_T	velocity of rotor blade
U_x	axial mean velocity
v	fluctuating velocity in the circumferential direction

LIST OF SYMBOLS (Cont'd)

$\rho_{uu}(\tau)$ $\overline{u\,(x,r,\theta,t)\;u\,(x,r,\theta,t+\tau)}\,/\sqrt{u^2}$

$\rho_{vv}(\theta)$ $\overline{v\,(x,r,t,\theta)\;v\,(x,r,t,\theta+d\theta)}\,/\sqrt{v^2}$

ϕ flow coefficient U_x/U_T

τ delay time (seconds)

LIST OF TABLES

LIST OF FIGURES

LIST OF FIGURES (Cont'd)

INTRODUCTION

Turbulence is an important cause of noise generation in aircraft turbomachinery (propellers, fans and compressors) as well as marine vehicles (propulsors and ventilation fans). The interaction of turbulence with the potential flow field of the rotor results in quadrupole noise sources. Dipole sources result from the random fluctuations in pressure distributions caused by the random fluctuations in the angle of attack due to the turbulence.

Recent investigations [1,2] have revealed that inlet turbulence, both in the free-stream and hub or annulus wall boundary layers, is a major source of noise in compressors, fans, and propulsors. Additional turbulence is generated in the wakes of inlet guide vanes (aircraft) or control surfaces (marine). In one of these earlier studies, [2], a detailed investigation of the radiated sound due to nearly isotropic turbulence interacting with a rotor was carried out. The aim of the investigation was to find the empirical relationship between turbulence intensity and the radiated sound power. A second aim was to check the validity of theories developed by Mani [3] and Sevik [4] to predict the radiated sound due to isotropic and homogeneous turbulence.

A review of the major sources of turbulence and its effect on noise in aircraft, marine and industrial turbomachinery as well as an up-to-date review of the various theoretical and experimental investigations is described in [5]. A more general review of all sources of noise is given in [6].

The relationship between the inlet turbulence properties (such as intensity, length scales and energy spectrum) and the radiated sound is not fully understood. The objective of this research program is to carry out a systematic study to

determine experimentally how the radiated sound depends on these turbulence
characteristics. This study has been carried out for three different inlet
boundary layers at the design flow coefficient of the turbomachine, and at
three flow coefficients with one type of boundary layer, all with and without
a grid. Two rotor solidities were considered and both the near and far-field
radiated sound were studied. The operating variables have provided a wide
range of turbulence eddy sizes leading to an understanding of the role played
by the turbulence integral scale on noise generation.

TURBOMACHINERY NOISE FACILITY

An existing aeroacoustic facility, as described in [2] was modified
by adding a long inlet duct and stationary hub to permit formation of a boundary
layer. The facility consists of four main components: an anechoic chamber
surrounding the inlet, the test rotor, an acoustical baffle chamber downstream of
the rotor, and a Joy axial flow fan to provide airflow. A detailed drawing
of the assembly is shown in Figure 1.

The anechoic chamber has inside dimensions of 3.35 x 3.66 x 2.44 m.
Construction is a wooden frame with walls much like a bookcase; the spaces
between the shelves being filled with Owens-Corning Type 705, industrial fiber-
glas. The floor is covered with the same material. Fiberglas is suspended
from the frame in wire baskets forming the ceiling. The fiberglas treatment
is 15.23 cubic inches thick with a one-inch airspace betwen the fiberglas and
exterior wall. The rotor inlet protrudes 0.38 meters through the center of a
3.35 m x 2.44 m wall. An air inlet hole, 1.4 m in diameter was cut in the
opposite wall and covered with a sheet of porous plastic foam to filter out
dirt. The chamber was calibrated in the above configuration by driving a
speaker with pure tones between 0.1 and 20 kHz. The variation of sound

pressure level with distance from the centerline of the inlet follows the inverse square law. The results indicate the chamber is anechoic over the range tested.

Two rotors were employed in the investigation; one having 10 blades, and one having 17 blades. Each rotor had identical blades with two differing solidities. The hub-to-tip ratio of the rotor blades is 0.482, with a tip diameter of 17.53 cm. The chord length is nearly constant from hub to tip at 4.06 cm. The stagger angle varies from 0.31 radians at the hub to 0.81 radians at the tip. The rotor is of free vortex design. The midspan blade spacing for the 17 and 10-bladed rotors are 2.43 cm and 4.13 cm, respectively. The range of mean velocities at the rotor inlet was 39.0 to 51.2 m/sec. At design, the lift coefficient for the 17-bladed rotor is 0.46 and the flow coefficient is 0.75.

A plot of experimentally determined C_L vs radial position is given in Figure 2. The operating conditions were as follows: ϕ = 0.629 at 6810 rpm and 39.3 m/sec, ϕ = 0.75 at 5440 rpm and 39 m/sec, and ϕ = 0.871 at 5440 rpm and 51.2 m/sec. C_L is for the 17-bladed rotor.

EXPERIMENTAL METHOD AND INSTRUMENTATION

Aerodynamic Measurements

Measurements of the mean velocity and the turbulence intensity in both the axial and tangential directions at the inlet were made with an x-configuration hot-wire probe. Standard data acquisition techniques, were used in conjunction with a correlation computer and spectrum analyzer, to derive turbulence characteristics. The recorded ac signals are accurate down to dc values,

since there was no signal filtering. Hence, the correlation measurements are accurate, including the calculation of long length scales. The probe was traversed radially along the blade span; measurements were taken at different radial locations at a position two chord lengths upstream of the rotor (as shown in Figure 3). Mean velocity measurements were made at 90 and 180 degrees separation from the main measuring station in order to determine if the flow was axisymmetric. The entry flow is axial everywhere upstream of the rotor.

The axial velocity and, thus flow coefficient, was controlled by the Joy axial flow fan, located downstream of the rotor as shown in Figure 1. An artificial boundary layer (ABL) was created by tripping it with a 0.318 cm thick 0-ring on the hub immediately behind the nose cone. In addition, a fully developed boundary layer (FDBL) was produced by coating the hub with rough sandpaper and removing the nose cone. The turbulence properties were altered by placing a square mesh grid at the inlet 3.5 diameters upstream of the rotor, see Figure 3. The grid had a mesh size of 2.86 cm and a rod diameter of .556 cm. Experiments were carried out with and without this grid. The axial length scales of the turbulence have been derived by using an x-array hot-wire probe in conjunction with a correlation computer and an x-y plotter to obtain auto-correlation curves for the axial component of the velocity fluctuations. Then, using the equation:

$$\int_0^\infty \rho_{uu}(\tau) \; d\tau = T \tag{1}$$

the temporal integral scale was derived from the autocorrelation curve.
This time scale multiplied by the local axial velocity gives the axial
integral length scale (L_x).

The circumferential length scales were determined by using two x-array
hot-wire probes whose angular separation could be varied. The cross-correlation
between the circumferential components at various angular separations, with
axial and radial location held constant, of the hot-wire probes was computed
with the correlation computer and plotted as correlation coefficient normalized
by $\overline{v^2}$ versus angular separation in degrees.

The integral length scales were derived from this plot using the equation:

$$r \int_0^\infty \rho_{vv}(\theta) \, d\theta = L_\theta \qquad (2)$$

The length scales were determined at each of five radial positions for
all three boundary layers at the design flow coefficient, with and without
the grid installed. In addition, turbulent energy spectra were obtained for both
the axial and circumferential components of the fluctuating velocity at each
radial location. It is assumed that the inflow turbulence characteristics
do not change with rotor geometry, and hence no turbulence measurements
were carried out for the 10-bladed rotor.

Acoustic Measurements

Measurements of the radiated sound were made at two locations, two chords
upstream of the rotor, called here the nearfield, and 4.35 duct diameters upstream
of the inlet duct opening inside the anechoic chamber, labeled the far field,
as shown in Figure 3. The near-field measurements were made with the micro-

phone mounted flush in the wall of the duct. The sound spectra were obtained

by analyzing the 1/4-inch B&K microphone signal through a Spectral Dynamics

real-time spectrum analyzer and recorded with an x-y plotter.

Spectra were obtained for three different flow coefficients, 0.75, 0.871,

and 1.03, without the grid for one boundary layer and for three different

boundary layers at the design flow coefficient (ϕ = 0.75) with and without

the grid. All sound measurements were performed with the 10-bladed, as well as

the 17-bladed rotor configurations.

Because of the length of the duct and its possible influence on sound

propagation, calibration of the acoustic response of the duct for all duct

configurations was performed. The results were identical for every configu-

ration. The sound spectra have not been corrected for the duct acoustic

response.

The variables used in the experimental program and the measurement program

for each of the variables are shown in Table I. The design flow coefficient

ϕ = 0.75 corresponds to an inflow velocity of 39 m/s. The rotor was operated

at a constant speed of 5440 rpm for all operating conditions.

Table I. Experimental Variables and BPF Tone Levels

Number of Blades	Boundary Layer	Grid	Flow Coefficient	U_c m/sec	Far-Field 10-bladed BPF Tone Level SPL (dB)	17-bladed BPF Tone Level SPL (dB)
17	Natural	No	1.03	51.5	-----	79
17	Natural	No	0.871	43.5	-----	79
10, 17	Natural	No	0.75	39.0	81.4	79
10, 17	Natural	Yes	0.75	39.0	79.4	74.7
10, 17	Artificial	No	0.75	39.9	79.0	79.9
10, 17	Artificial	Yes	0.75	39.9	74.4	74.2
10, 17	Fully Dev.	No	0.75	39.5	84.7	82.7
10, 17	Fully Dev.	Yes	0.75	39.5	75.3	80.0

August 27, 1976
                                        NM:BL:DET:mac

EXPERIMENTAL RESULTS

Aerodynamic Measurements

The results of axial mean velocity measurements are shown in Figure 4.
The artificial boundary layer, ABL, is seen to have nearly the same thickness
as the natural boundary layer, NBL, but has a much steeper gradient at the hub.
The fully developed boundary layer, FDBL, is much thicker than either the NBL or
ABL. A logarithmic plot of velocity profile seems to indicate that all
three boundary layers obey the law of the wall.

In Figures 5 and 6, the turbulence intensity profiles are shown for all
three boundary layers. The levels increase with increasing boundary layer
thickness, with the maximum intensities for FDBL case. The turbulence intensities
with the grid are generally higher. For the NBL, the tangential component of
turbulence is much lower than the axial component. For the ABL and FDBL, the
two components of turbulence intensity are nearly the same for the middle third of
the passage. The tangential component is lower than the axial component inside
the hub and annulus wall boundary layers. Hanson's measurements [1] indicate that,
for a fan operating in atmospheric turbulence, the contraction at the inlet would
result in larger values of the tangential component of turbulence intensity than
of the axial component. In the present case, the eddies are contracted as they
are sucked through an opening in the wall of the anechoic chamber, as shown in
Figure 1, expanded inside the chamber and contracted again at the inlet of the
fan. This would probably account for the discrepancies between Hanson's [1]
and the present measurements.

For the axial component of the velocity fluctuations, two length scales were found to exist simultaneously for the no grid condition for all three boundary layers. Figure 7a is a typical autocorrelation curve with no grid installed showing evidence of two length scales and how they were determined. This evidence also appears in the circumferential spatial cross-correlation with the grid, it disappears for the autocorrelation (see Figure 7b). This indicates that the grid reduces the axial length scale drastically, but has no effect on the circumferential length scale.

In Table II, the axial length scales found at five radial locations are given for each of the three boundary layers. It is readily seen that two scales were found at all locations for the no grid condition except for two locations for the FDBL.

The NBL shows the greatest uniformity for axial length scales with no grid installed. The FDBL shows the greatest variation. These variations are smoothed out by the installation of the grid. All three boundary layers have axial scales of the same order of magnitude with the grid installed. Table II also gives the average axial integral length scales. These scales were derived using Equation 1 as previously discussed. Instead of splitting the autocorrelation curve into two curves as shown in Figure 7a, the entire autocorrelation curve was integrated.

Table III gives the circumferential length scales at five radial locations for all three boundary layers. Two scales were present for all locations and boundary layers, however, not all could be calculated. Hanson [1] found L_x to be over 30 m, while he measured an L_θ of only 7.6 cm at mid-span. This compares to an average of 90 cm for L_x and an L_θ of 10 cm (large) and 0.12 cm (small) in the Natural Boundary Layer.

Table II Axial Integral Length Scales (cms)

Natural Boundary Layer (NBL)

r/r$_T$	No Grid			Grid
	Long	Short	Average	
0.52	86	10	46	1.5
0.61	68	7	42	2.2
0.75	90	9	77	1.9
0.88	97	12	68	2.2
0.97	117	5	81	2.2

Artificial Boundary Layer (ABL)

0.52	386	69	321	1.9
0.58	121	14	74	1.7
0.70	84	13	54	0.9
0.84	194	45	160	1.0
0.97	152	40	112	3.2

Fully Developed Boundary Layer (FDBL)

0.52	164	21	112	2.1
0.58	NP	2	2	2.1
0.70	34	3	5	1.5
0.84	NP	1.4	1.4	0.4
0.97	85	13	70	1.0

NP = Not Present

Table III Circumferential Integral Scales (cms)

Natural Boundary Layer (NBL)

	No Grid		Grid	
r/r_T	Large	Small	Large	Small
.52	3.6	.07	2.1	.11
.61	9.2	.10	7.2	.15
.75	7.9	.17	7.0	.12
.88	12.2	.05	11.1	.35
.97	23.3	.17	8.0	.17

Artificial Boundary Layer (ABL)

.52	.50	.29	.32	.21
.58	.71	.29	.86	.21
.70	3.60	.48	3.10	.36
.84	.32	.45	.38	.17
.97	4.00	.39	ND	.14

Fully Developed Boundary Layer (FDBL)

.52	1.80	.34	1.80	.33
.58	1.20	NP	1.30	NP
.70	ND	.38	ND	.35
.84	1.10	NP	NP	.45
.97	6.10	.46	5.60	.43

NP = Not present
ND = Not determinable

Figures 8 and 9 show the correlation curves near the hub with various entry boundary layers at ϕ = 0.75 for r/r_T = 0.52 and 0.58, respectively. The autocorrelation, $\rho_{uu}(\tau)$, is shown only for the no-grid case and the cross-correlation for both the cases. The correlations are highly anisotropic in all these cases.

A possible explanation for the presence of two turbulence length scales is the fact that the eddies in the free stream are stretched as they are ingested into the inlet resulting in long, elongated eddies. Small scale eddies arise from the hub wall boundary layer and probably exist in the form of a ring vortex. Evidence of long eddies is clear from plots of $\rho_{uu}(\tau)$ in Figures 7a, 8 and 9 and Table II. The presence of the grid tends to reduce or eliminate the long eddies as seen in Figures 7b, 8, 9, and Table II.

With all three boundary layers, the cross-correlation ($\rho_{vv}(\theta)$) plots indicate the presence of a thin as well as a ring vortex type of eddy. In the artificial boundary layer, the cross-correlation becomes negative. This implies that the ring vortex eddy has changed its direction of rotation. Since this change in direction of rotation occurs at radial locations near the hub, it probably results from the "O" ring trip near the nose cone of the hub. The cross-correlation curves for the fully developed boundary layer are similar to the natural boundary layer. The grid does not seem to bring about any substantial change in the tangential extent or length of the eddies as seen in Figures 8, 9, and Table III.

The turbulent energy spectra were derived from the hot-wire measurements at five radial locations. When these are normalized by total turbulence intensity (integrated over all the wave numbers), the data at all the five radii band as shown in Figure 10, indicating that the energy spectrum is similar at all radii.

The slope of the axial component and the tangential component of intensity in the range 10 to 100 m^{-1} is found to be -2.6.

Acoustic Measurements

The spectrum of background noise was taken without rotor, but with and without the auxiliary fan in operation. The background is low enough not to effect the radiated noise from the rotor.

The results of the sound measurements show a definite dependence on turbulence length scales. In Figures 11 and 12, a comparison is made between the spectra obtained with the grid and no grid (far and near field) for the natural boundary layer for both 10 and 17 blades. The decrease in the number and strength of harmonics above the blade passing frequency, BPF, for the grid spectra is due solely to the large decrease in axial length scale caused by the grid. The small rise in broadband noise can be attributed directly to the increase in turbulent intensity due to the presence of the grid. In Figure 13, a comparison is made between the far-field noise spectra due to the 17 and 10-bladed rotors operating in the natural boundary layer configuration with no grid. The two spectra were normalized with respect to frequency using $f/B\Omega$, where f is frequency, B is number of blades, and Ω is rotor rps. The turbulence properties were measured only for the 17-bladed rotor. They were assumed to be the same for the 10-bladed rotor, since the operating conditions and blade geometries are identical for both rotors. Hence, the only changes in the two configurations is the blade spacing, and steady loading. The unsteady aerodynamic transfer function is dependent on the spacing and is approximately proportional to the slope of the C_L vs incidence curve. Hence, using the flat plate cascade theory, the increase in noise level shown in Figure 13 due to a change in

spacing can be estimated to be about 2 db at BPF. The remaining increase

for the 10-bladed rotor is presumably due to the change in L_x/S value with

L_x fixed and S changing. This seems to confirm, qualitatively, Mani's [3] conclu-

sion on the effect of L_x/S on noise level.

In Figures 14 through 17, the sound spectra for the two rotor configurations

are compared for the three different boundary layers. The corresponding BPF tone

levels are tabulated in Table I. A general increase in the broadband noise

level with increasing boundary layer thickness is attributed to the increase in

turbulence intensity for each boundary layer, and not to any mean velocity

gradient effect. The change in intensity between the NBL and ABL is not large,

while there is a substantial increase in intensity for the FDBL case (Figures 5

and 6).

The BPF tone is highest for the fully developed boundary layer. This is a

consequence of the higher levels of turbulence intensity associated with the

FDBL. Referring to Figures 11 and 12 and Tables II and III, it is apparent

that the axial length scale has more influence on the number and strength of the

higher harmonics of the BPF tone than on the strength of the BPF tone itself.

The turbulence intensity has a major influence on the BPF tone noise. Hence, a

small difference between the NBL and ABL BPF peaks is seen. The BPF noise level

is highest for FDBL case with ABL being the lowest of the three. Referring to

Tables II and III, it is evident that the ABL has the longest axial length

scale and shortest tangential length scale. The latter may have considerable

influence in providing the lowest noise level at BPF for the artificial boundary

layer. This seems to indicate the importance of tangential length scale (L_θ/S),

which is less than unity at most radii for ABL case.

Figure 18 shows the sound spectra for the natural boundary layer, no grid configuration, for three different flow coefficients, 0.75, 0.87, and 1.03. The broadband noise level rises with increasing flow coefficient, while the BPF tone is constant. The rise in broadband noise level is due to the increase in mean velocity and turbulence intensity associated with the increased flow coefficient. A change in flow coefficient corresponds to a change in steady blade loading. Figure 18 also indicates that changes in the steady blade loading affect the number of higher harmonics present.

CORRELATION AND DISCUSSION

Previous investigations, both theoretical and experimental, have indicated that the sound power varies as the square of the turbulence intensities and inversely as the square of the axial integral length scale for the rotor interacting with isotropic turbulence. In the present investigation, a different correlation has been found. The sound power still varies as the square of turbulence intensities, but inversely as the ratio of axial integral length scale to the blade spacing. With the 10-bladed rotor operating with the grid, the proper mean inflow velocities could not be achieved, hence the results do not appear in the correlations. The correlating parameter is $\overline{q^2}\, U^4_{rel}\, (L_x/S)^{-1}$, where $\overline{q^2}$ is the turbulence intensity normal to the blade, and L_x is the axial integral length scale. The far-field sound at BPF is correlated in Figures 19 and 20 and follows the relation:

$$SPL = (SPL)_0 + 40 \log U_{rel} + 10 \log \overline{q^2} - 10 \log L_x + 10 \log S \qquad (3)$$

where $(SPL)_0$ is a constant base level.

The values of the turbulence properties are taken from near the hub and near the tip. Correlations with values at mid-radius were poor. This indicates that sound generation is primarily from the root and tip regions of the rotor which operates in the hub and outer wall boundary layers.

The main effect of the long axial length scale is on the number and strength of higher harmonics of the BPF. This is clearly shown in Figures 11 and 12, where the sound spectra with and without the grid are compared. When the long scales were present (no grid), the second and third harmonics were present. When only the small scales are present (grid) these disappear. Hanson [1] reached a similar conclusion saying that the long length scales are responsible for the spectral distribution of sound energy, that is, they lead to narrow peaks in the noise spectra.

No definite conclusions can be drawn with regard to the effect of the tangential scales on the sound spectrum. An interesting observation is that the tangential scales, L_θ, for the ABL were much less than the blade spacing, S. The BPF levels for the ABL were lower than either the NBL or FDBL both of which had much higher L_θ/S ratios.

CONCLUSIONS

The following conclusions can be drawn from this study whose objective was an understanding of the relationship between boundary layer inflow turbulence and the noise generated by its interaction with a blade row.

1.   Two length scales of turbulence were found to exist simultaneously in the inflow of a static fan facility with no grid installed, long and short scales in the axial direction, narrow and wide in the tangential direction. The long axial scale disappears with a grid present.

2.   Turbulence intensities were found to be maximum at the outer wall with appreciable magnitudes found even at mid-radius where the turbulence is primarily from the free stream.

3.   The controlling factors in noise generation are the turbulence intensity and length scale.   An empirical relation (Equation 3) has been developed between these turbulence properties and radiated noise levels.   It does not seem to make any difference as to the source of the turbulence.   Boundary layer and atmospheric turbulence have the same effects.   Atmospheric turbulence does influence boundary layer turbulence.

4.   The long axial length scales appear to be a strong factor in determining the number and strength of BPF harmonics.   Short axial length scales contribute primarily to the general broadband noise levels.   These major differences between the effect of long and short length scales seem to account for the discrepancies between inflight and static noise tests.

5.   The primary sources of sound radiated from the rotor appear to be the root and tip regions.   Since these regions often operate in boundary layers, boundary layer turbulence can be an important source of radiated noise.

6.   Mani's [3] prediction that with decreasing L_x/S (for nearly isotropic turbulence), the general noise level will increase and BPF peaks will broaden seems to be borne out by the comparison between 17- and 10-bladed rotor spectra with identical entry turbulence.

7. The measurements indicate that the noise level, particularly at BPF, depends on the tangential scales, but no quantitative conclusions could be drawn.

8. Changes in the blade loading affect the number of BPF tones present in the sound spectrum.

REFERENCES

1. Hanson, D. B., "Spectrum of Rotor Noise Caused by Atmospheric Turbulence," Journal of Acoustical Society of America, Vol. 56, No. 1, July 1974.

2. Robbins, B. and Lakshminarayana, B., "Effect of Inlet Turbulence on Compressor Noise," Journal of Aircraft, Vol. II, No. 5, pp. 273-281, 1974.

3. Mani, R., "Noise Due to Interaction of Inlet Turbulence with Isolated Stators and Rotors," Journal of Sound and Vibration," Vol. 17, No. 2, pp. 251-260, 1971.

4. Sevik, M., "Sound Radiation from a Subsonic Rotor Subjected to Turbulence," in Fluid Mechanics, Acoustics, and Design of Turbomachinery, Edited by B. Lakshminarayana, W. R. Britsch, and W. S. Gearhart, NASA SP 304, Part 2, pp- 493-511, 1976.

5. Lakshminarayana, B., "Influence of Turbulence on Fan Noise," Proceedings of the Workshop on "Ventilation System Cooling Fan Noise," Naval Sea Systems Command. Edited by M. Sevik and J. Pierpoint, 1976.

6. Feiler, C. E., Conrad, E. W., "Fan Noise from Turbofan Engines," Journal of Aircraft, Vol. 13, No. 2, pp. 128, February 1976.
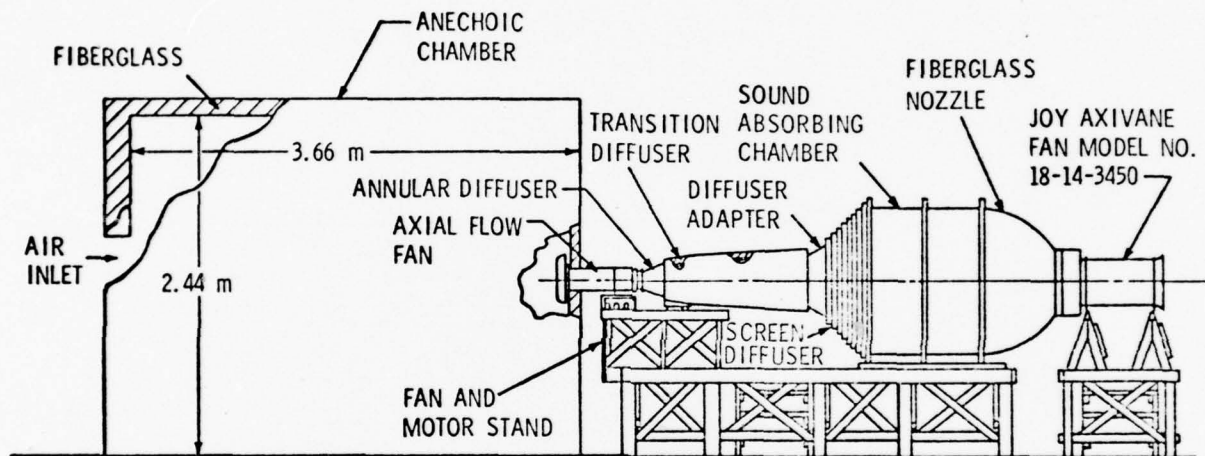
Figure 1 – Turbomachinery Noise Facility and Semi-Anechoic Chamber
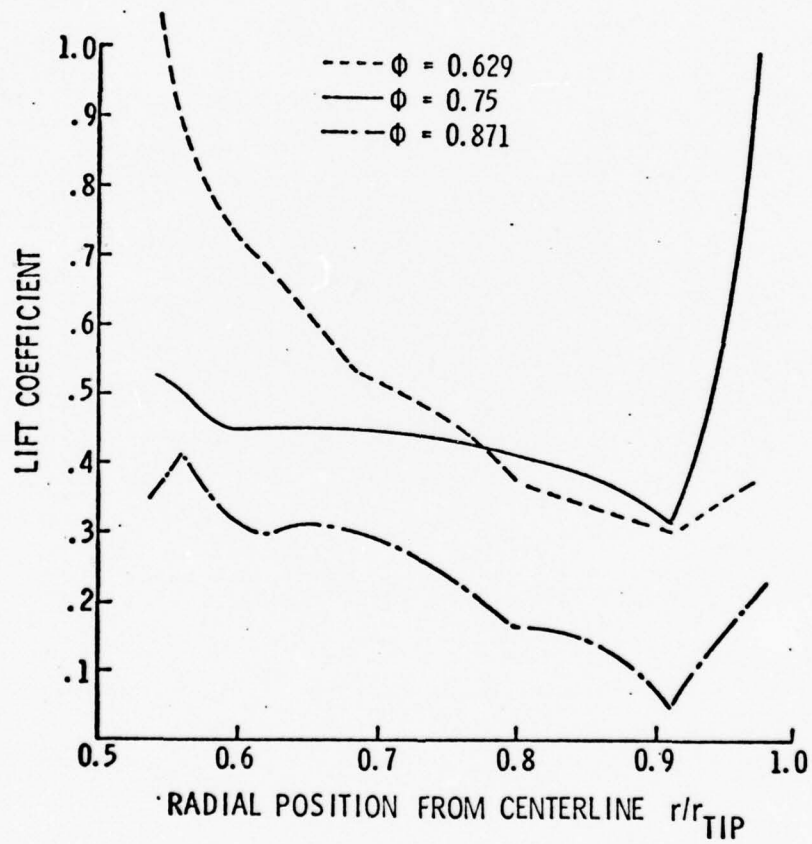
Figure 2 - Lift Coefficient vs Radial Position

2
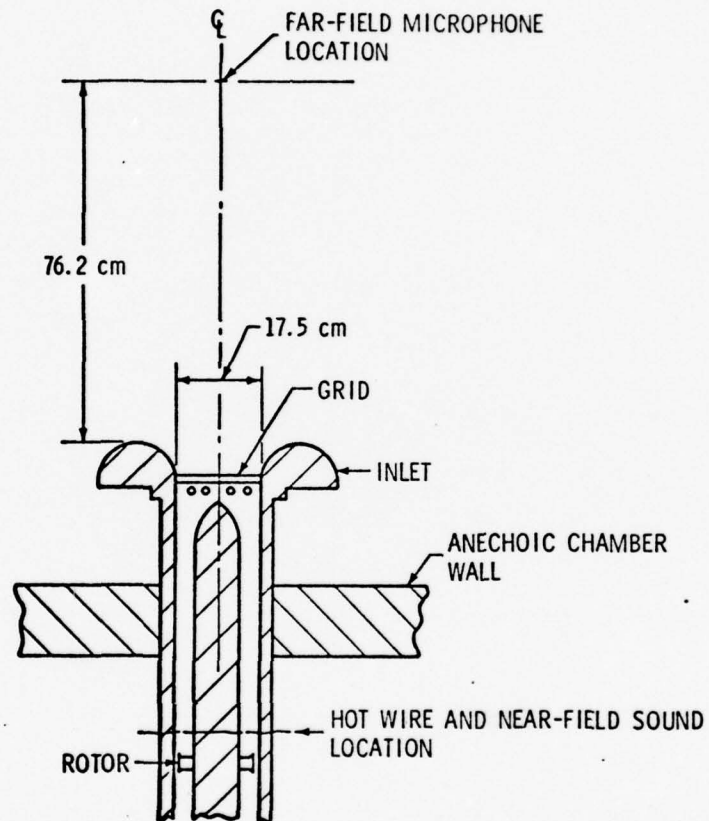
Figure 3 - Plan View of Inlet Showing Measuring Stations
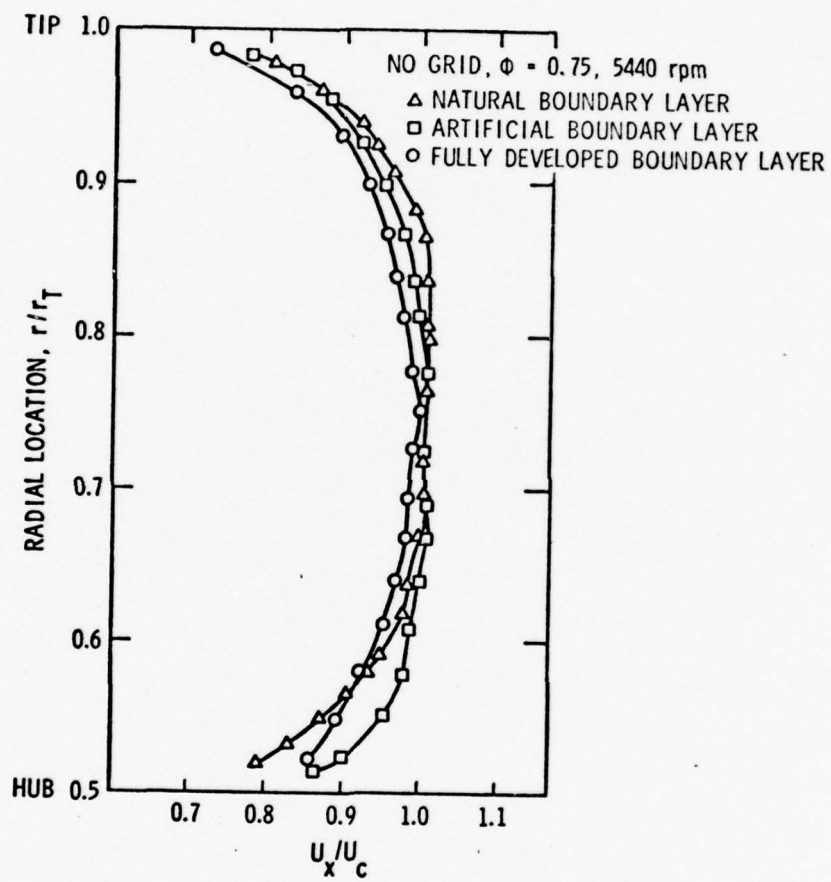
Figure 4 - Mean Axial Velocity Profiles
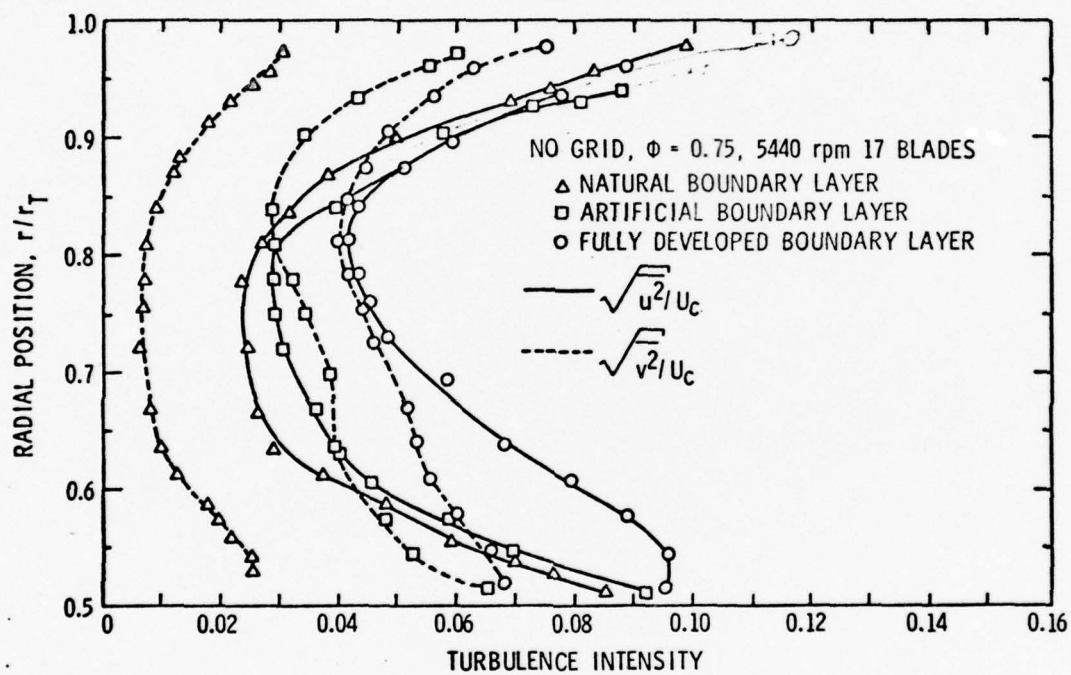
Figure 5 – Turbulence Intensity Profiles – No Grid Installed
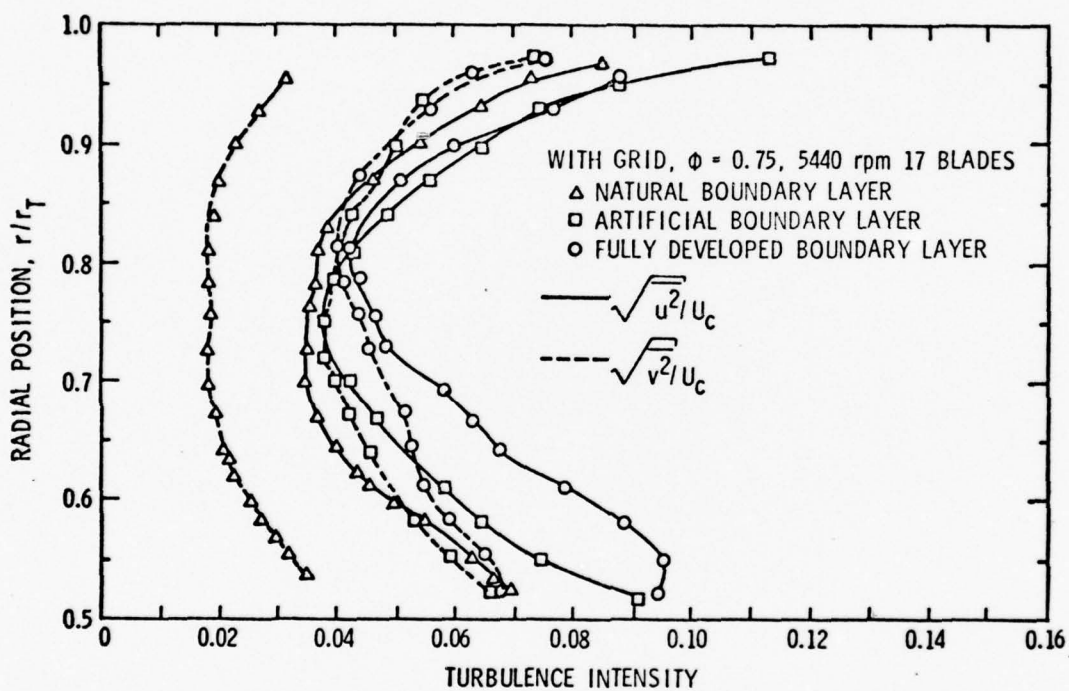
Figure 6 - Turbulence Intensity Profiles - Grid Installed

NO GRID, NBL
$r/r_T = 0.61$
$\Phi = 0.75$
17 BLADES
5440 rpm

SHORT EDDY

LONG EDDY

AUTO CORRELATION FUNCTION, $\rho_{uu}(\tau)$

TIME DIFFERENCE (msec)
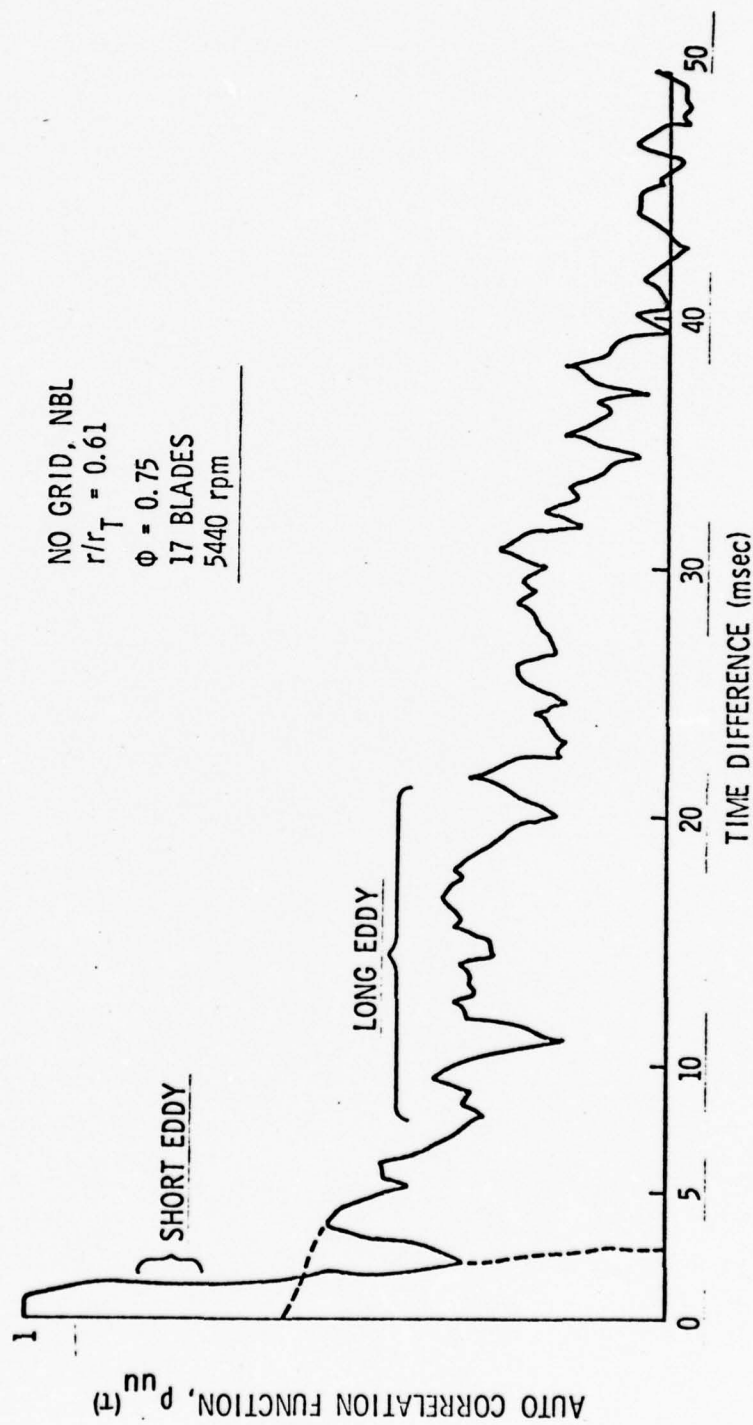
Figure 7a - Typical Autocorrelation Curve for No Grid Showing Two Scales

7b
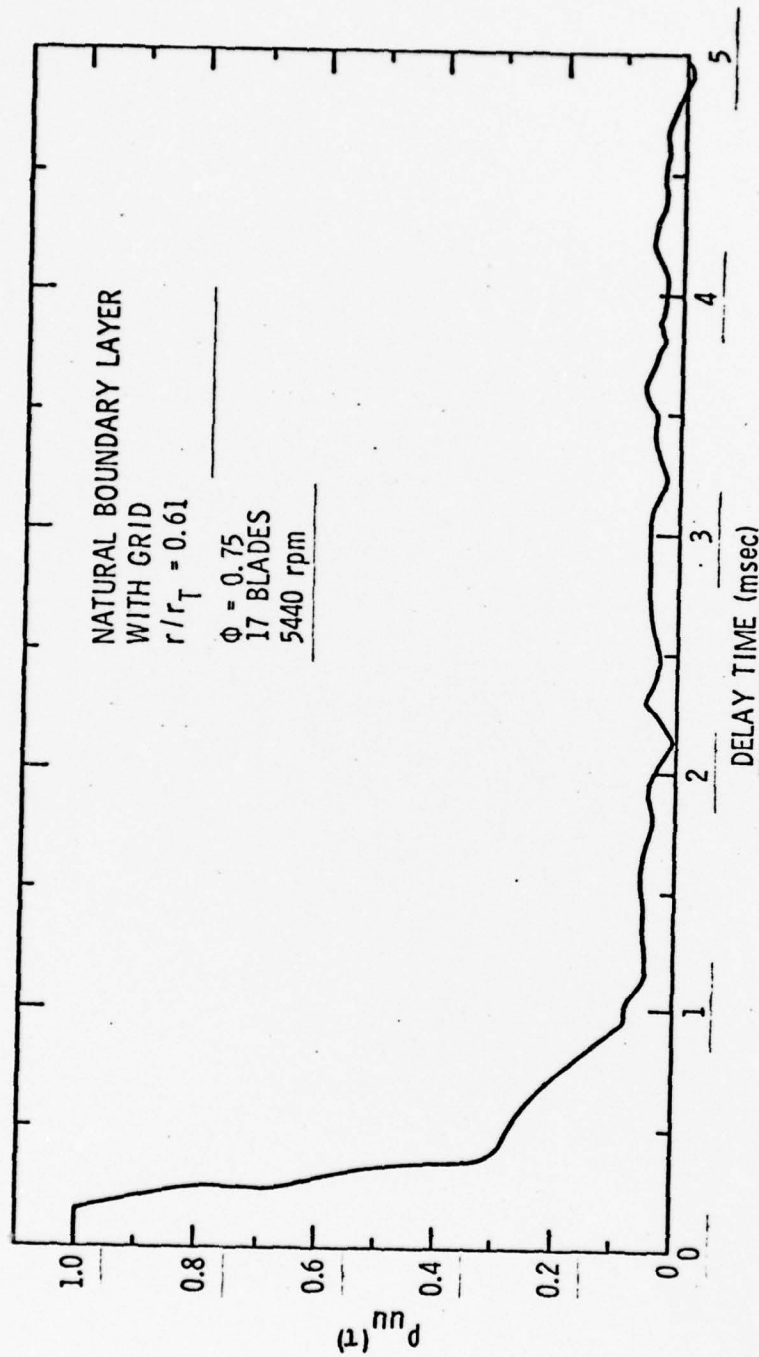
Figure 7b - Typical Autocorrelation Curve for Grid Installed
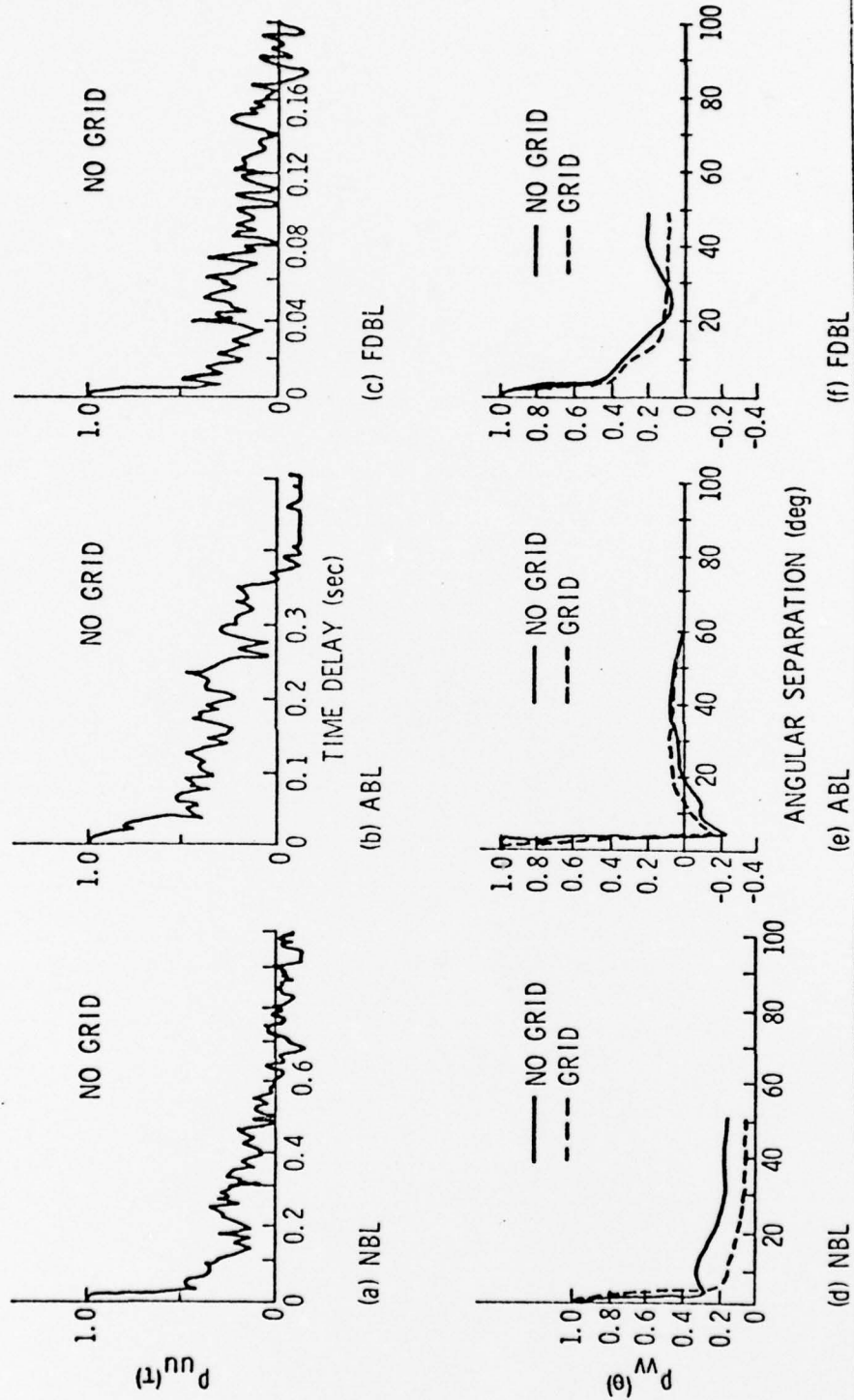
Figure 8 — Correlation Curves, Each Boundary Layer $r/r_T = .52$, $\phi = 0.75$, 17 blades, 5440 rpm
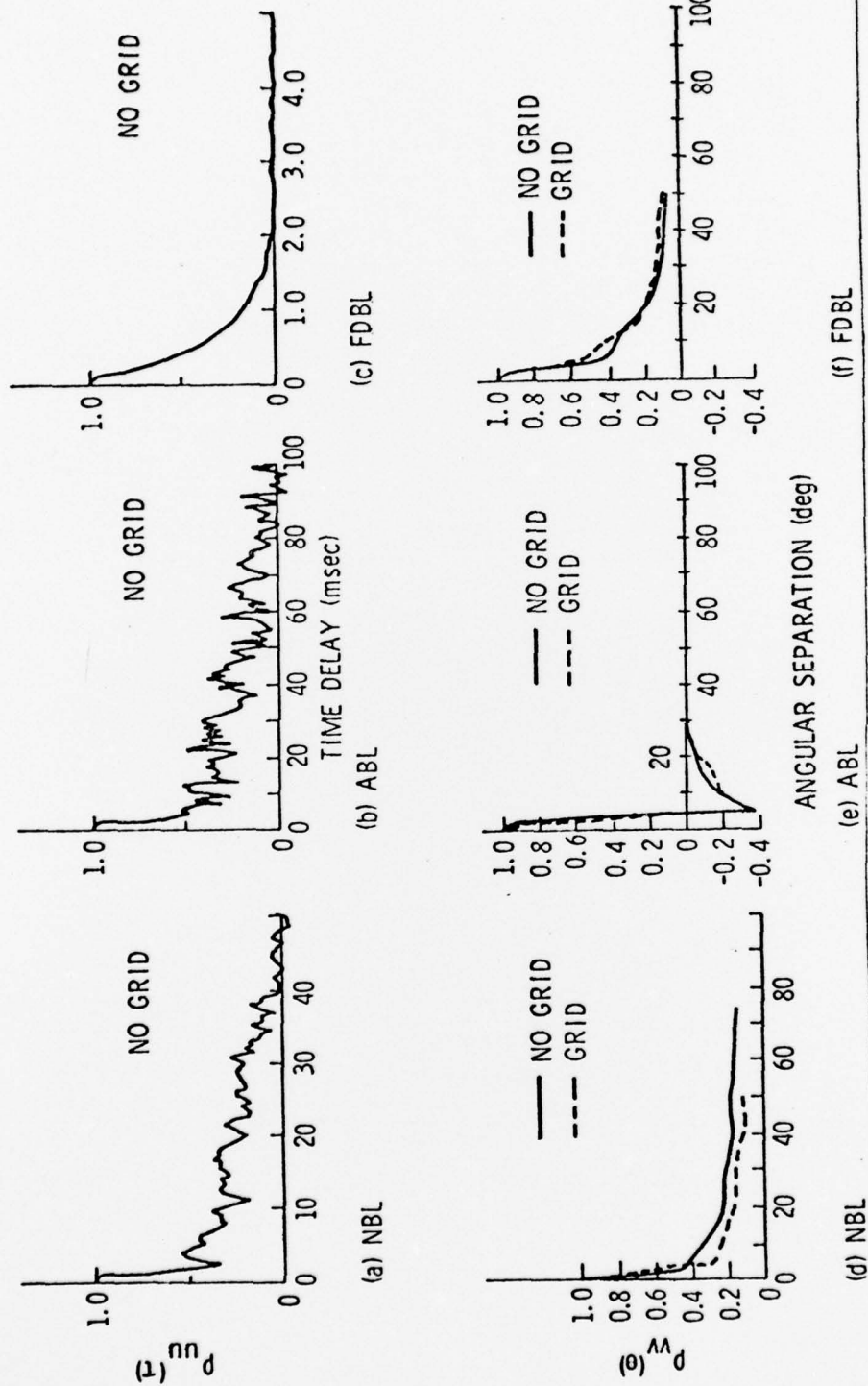
Figure 9 - Correlation Curves, Each Boundary Layer, r/r_T = .58, ϕ = 0.75, 17 blades, 5440 rpm
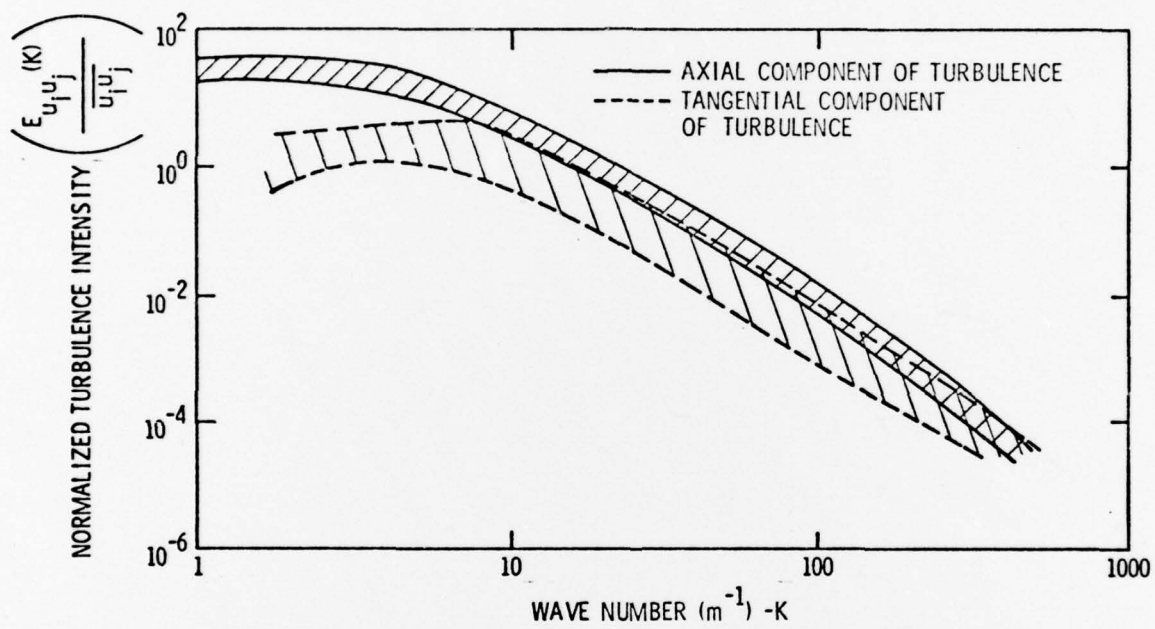
Figure 10 - Normalized Turbulent Intensity Curves
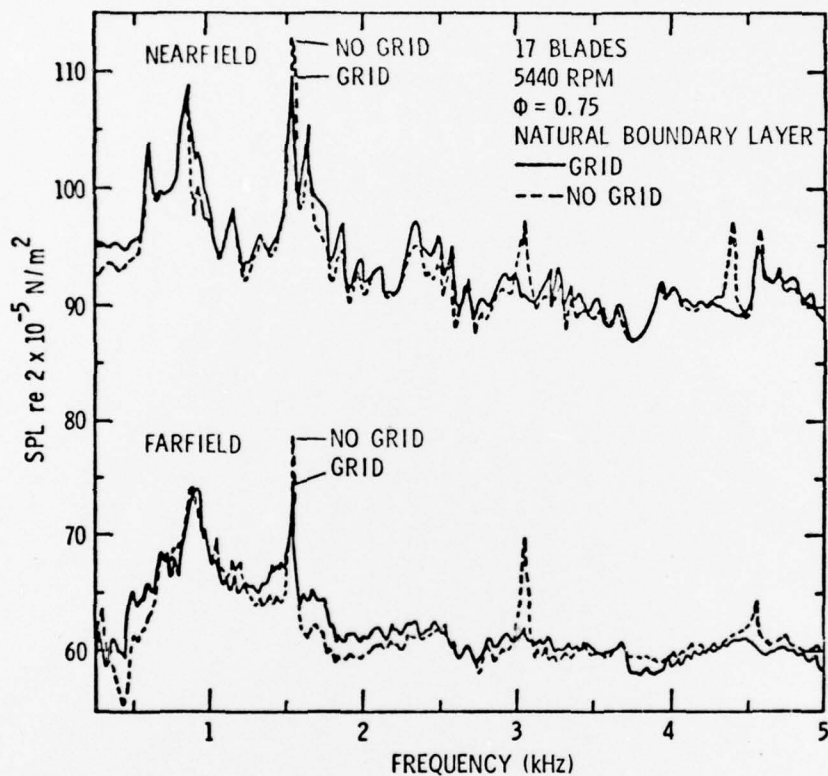
Figure 11 - Comparison of 17-Bladed Sound Spectra with and
Without Grid
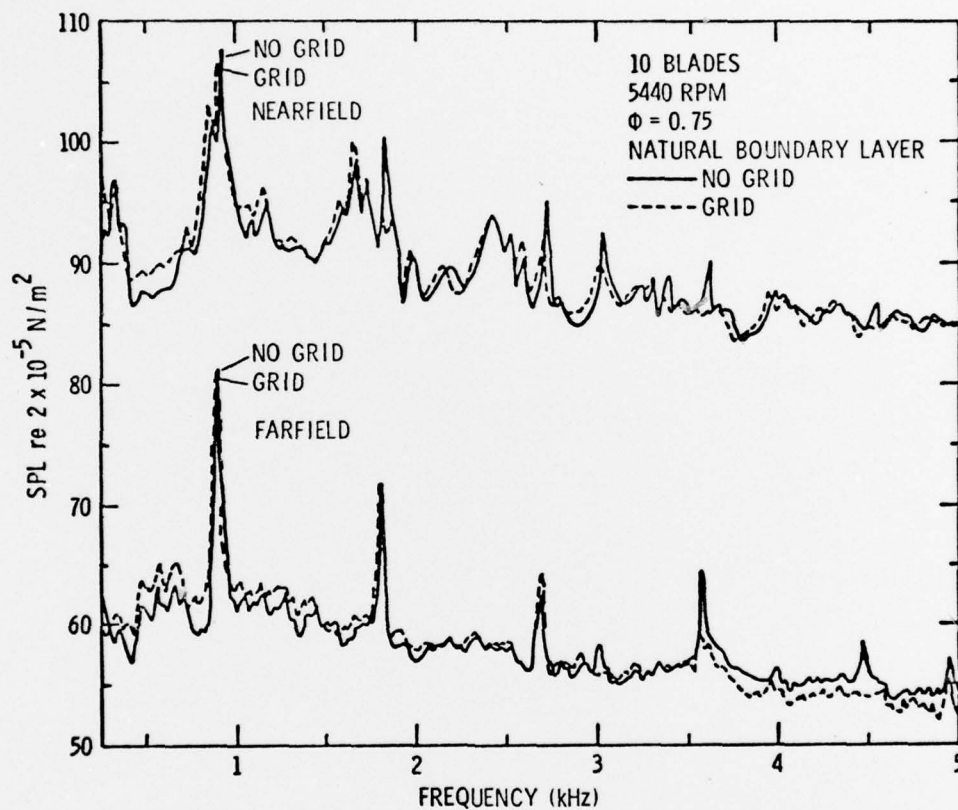
Figure 12 - Comparison of 10-Bladed Sound Spectra With and
Without Grid
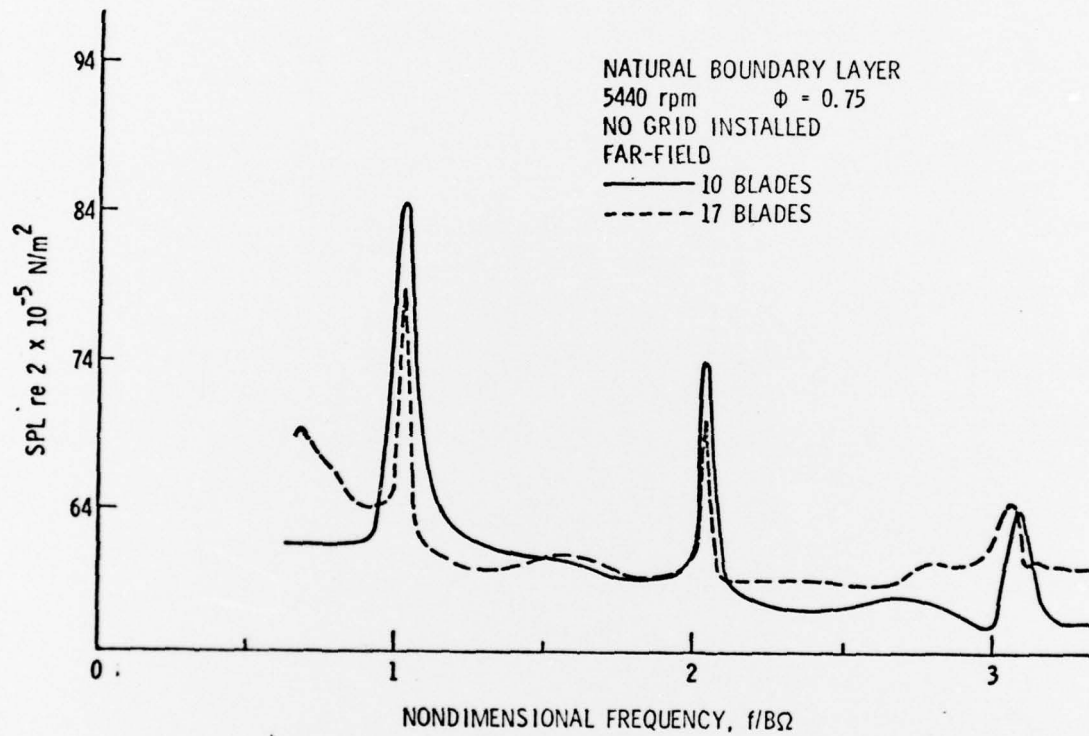
Figure 13 - Comparison of 17 and 10-Bladed Sound Spectra Without Grid
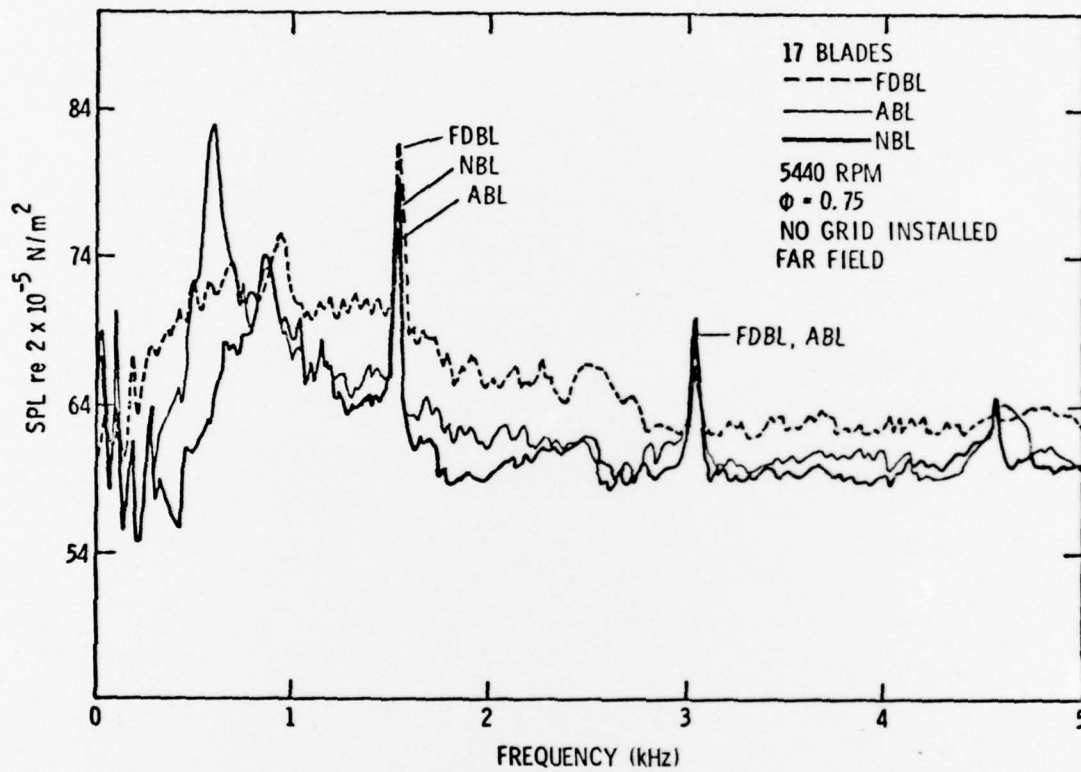
Figure 14 - Comparison of 17-Bladed Sound Spectra for all Three
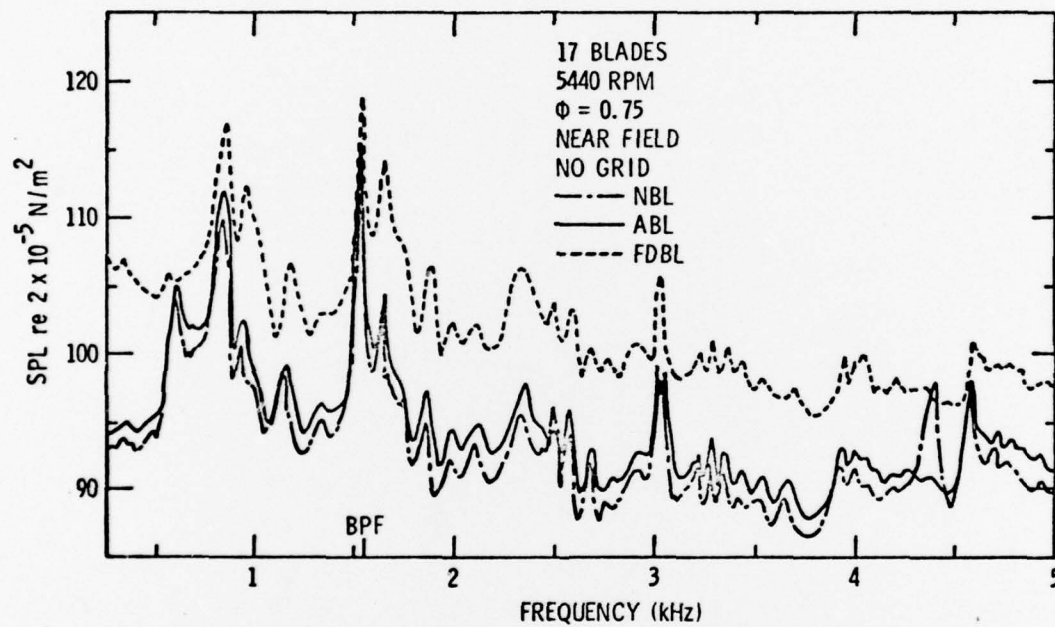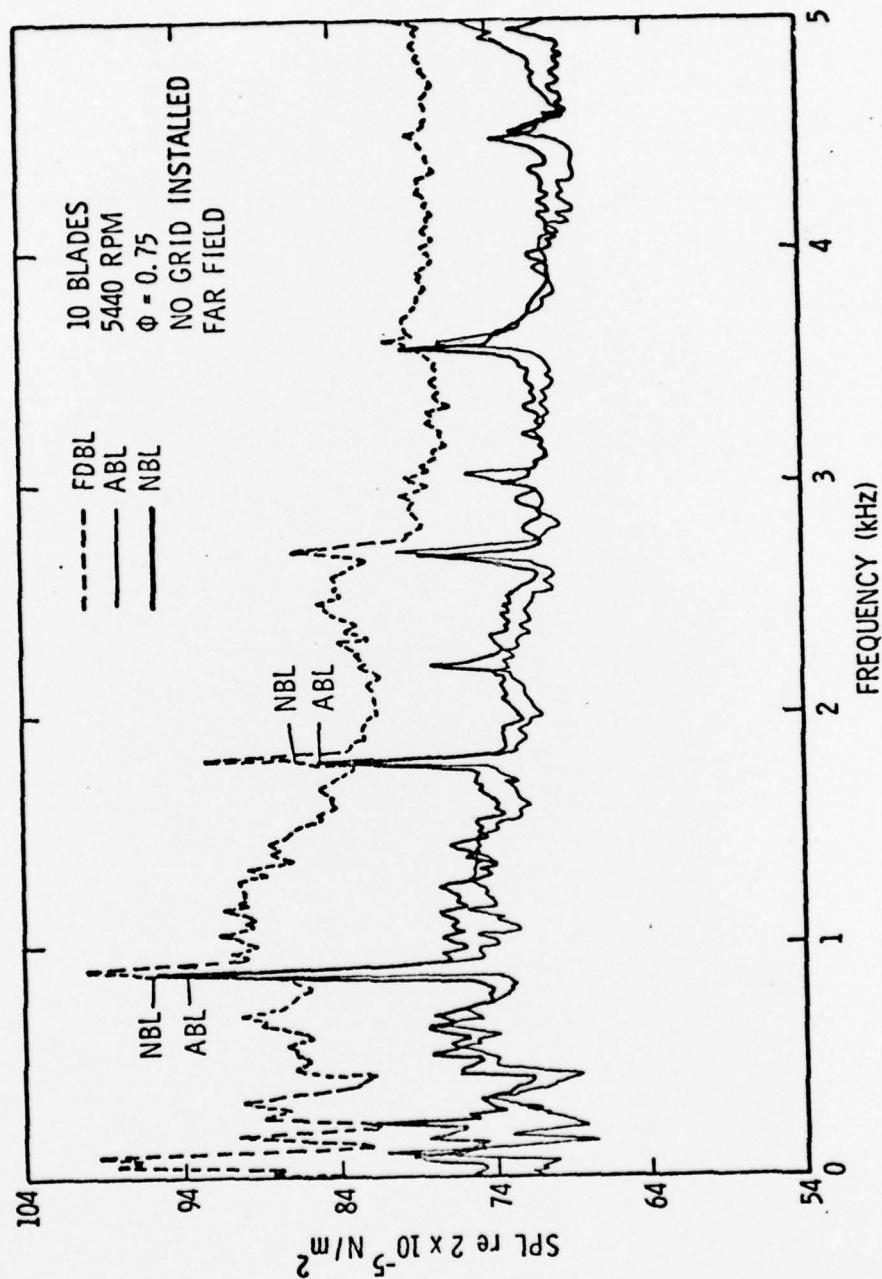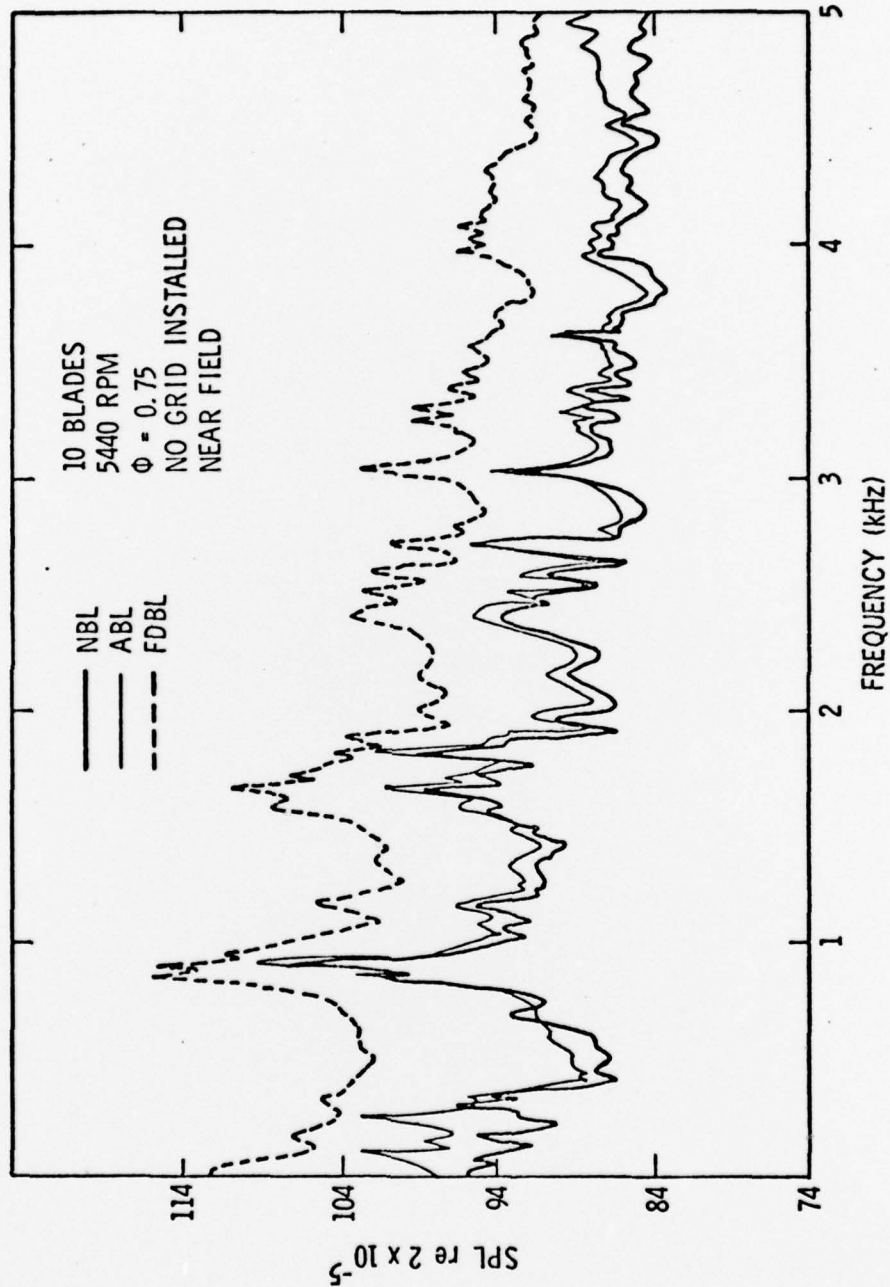Boundary Layers (Far-Field)

Figure 15 - Comparison of 17-Bladed Sound Spectra for all
Three Boundary Layers (Near-Field)

Figure 16 - Comparison of 10-Bladed Sound Spectra for all Three
Boundary Layers (Far-Field)

Figure 17 - Comparison of 10-Bladed Sound Spectra for all Three
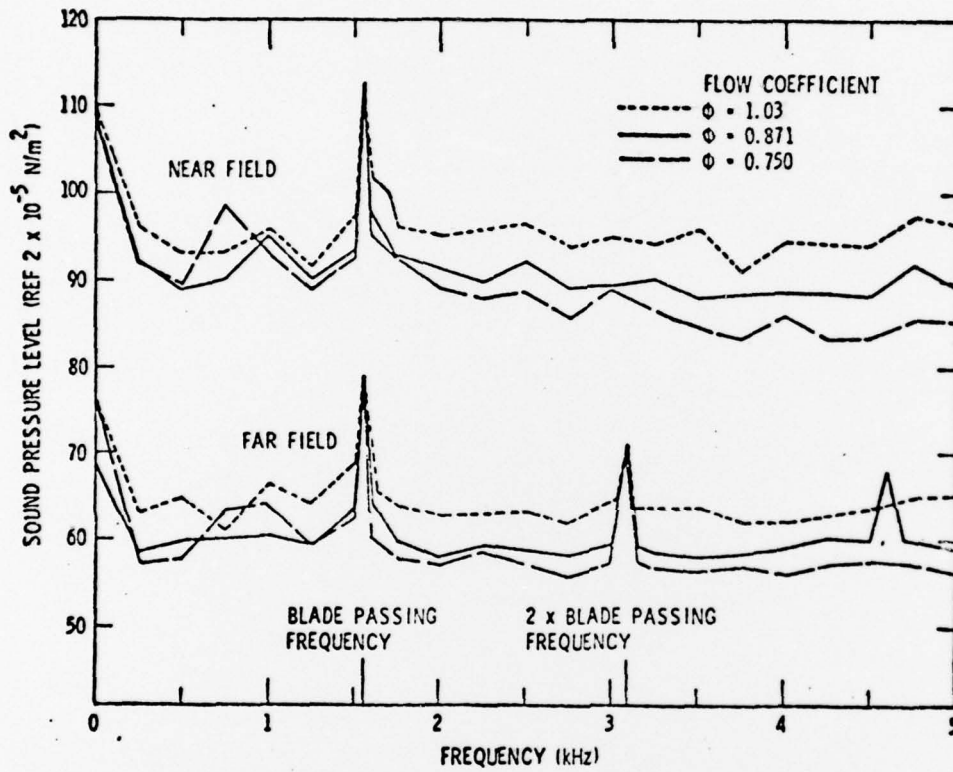Boundary Layers (Far-Field)

Figure 18 – Comparison of 17-Bladed Sound Spectra for
Three Different Flow Coefficients for the
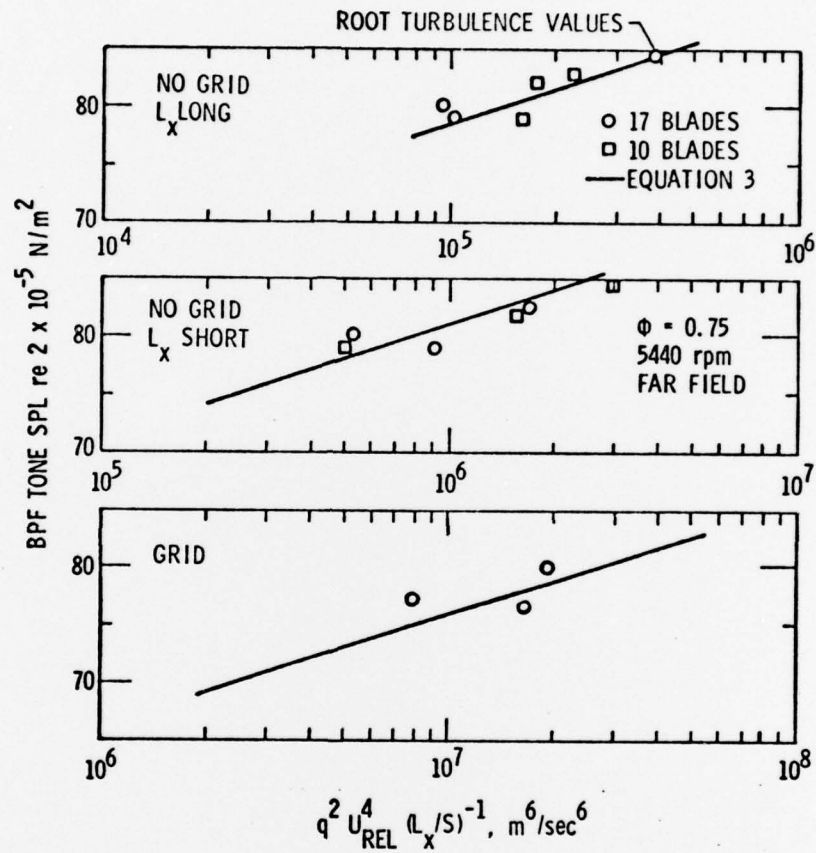Natural Boundary Layer

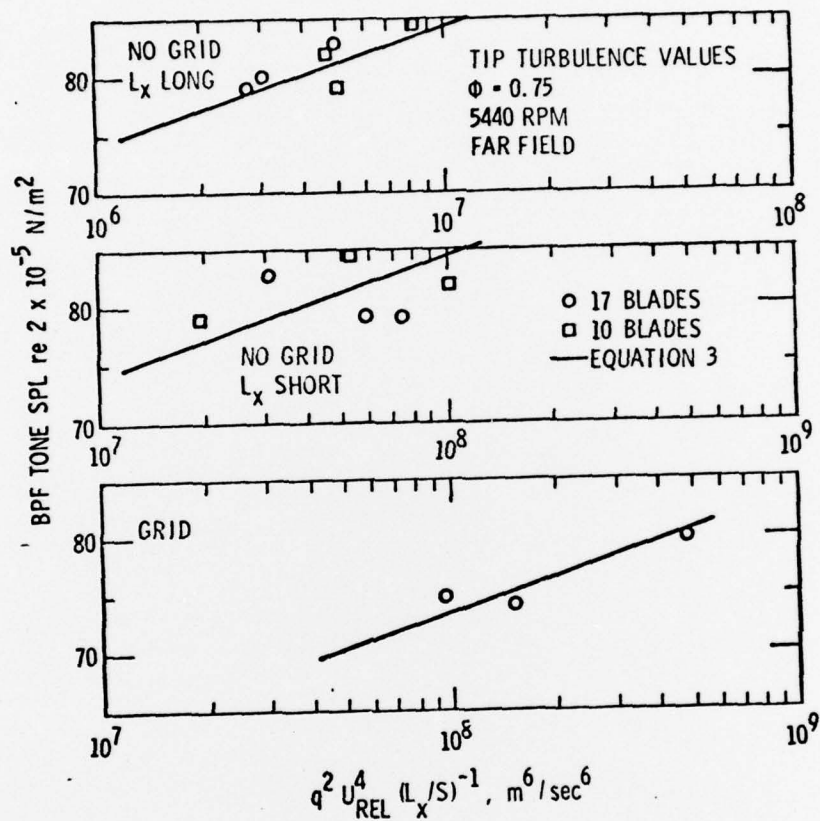Figure 19 - Correlation Between Noise and Turbulence
Data (Root Values)

Figure 20 – Correlation Between Noise and Turbulence Data
(Tip Values)

DISTRIBUTION LIST FOR UNCLASSIFIED TM 76-241 by N. Moiseev, B. Lakshminarayana, D. E. Thompson, dated August 27, 1976

Commander
Naval Sea Systems Command
Department of the Navy
Washington, DC 20362
Attn: Library
      Code NSEA-09G32
(Copy Nos. 1 and 2)

Naval Sea Systems Command
Attn: T. E. Peirce
      Code NSEA-0351
(Copy No. 3)

Naval Sea Systems Command
Attn: H. C. Claybourne
      Code NSEA-0371
(Copy No. 4)

Naval Sea Systems Command
Attn: A. R. Paladino
      Code NSEA-0372
(Copy No. 5)

Commanding Officer
Naval Undersea Center
San Diego, CA 92132
Attn: D. Nelson
      Code 2542
(Copy No. 6)

Commanding Officer & Director
David W. Taylor Naval Ship R&D Center
Department of the Navy
Bethesda, MD 20084
Attn: S. F. Crump
      Code 1505
(Copy Nos. 7 - 16)

David W. Taylor Naval Ship R&D Center
Attn: W. B. Morgan
      Code 154
(Copy No. 17)

David W. Taylor Naval Ship R&D Center
Attn: R. Cumming
      Code 1544
(Copy No. 18)

David W. Taylor Naval Ship R&D Center
Attn: J. McCarthy
      Code 1552
(Copy No. 19)

David W. Taylor Naval Ship R&D Center
Attn: T. Brockett
      Code 1544
(Copy No. 20)

David W. Taylor Naval Ship R&D Center
Attn: M. Sevik
      Code 19
(Copy No. 21)

David W. Taylor Naval Ship R&D Center
Attn: W. Blake
      Code 1942
(Copy No. 22)

Defense Documentation Center
5010 Duke Street
Cameron Street
Alexandria, VA 22314
Via: Commander (SEA-09G32)
     Naval Sea Systems Command
     Department of the Navy
     Washington, DC 20362
(Copy Nos. 23 - 34)

Dr. B. Lakshminarayana
Department of Aerospace Engineering
The Pennsylvania State University
233 Hammond Building
University Park, PA 16802
(Copy No. 35)

Dr. D. E. Thompson
Applied Research Laboratory
The Pennsylvania State University
P. O. Box 30
State College, PA 16801
(Copy No. 36)

Garfield Thomas Water Tunnel Library
Applied Research Laboratory
The Pennsylvania State University
P. O. Box 30
State College, PA 16801
(Copy No. 37)